ADVANCING EARTH AND SPACE SCIENCES

Geophysical Research Letters

RESEARCH LETTER
10.1029/2024GL112774

Links Between Internal Variability and Forced Climate Feedbacks: The Importance of Patterns of Temperature Variability and Change

Luke L. B. Davis[1,2], David W. J. Thompson[1,2], Maria Rugenstein[2], and Thomas Birner[3,4]

[1]School of Environmental Sciences, University of East Anglia, Norwich, UK, [2]Department of Atmospheric Science, Colorado State University, Fort Collins, CO, USA, [3]Meteorological Institute, Ludwig-Maximilians-University, Munich, Germany, [4]Institute for Physics of the Atmosphere, Deutsches Zentrum für Luft- und Raumfahrt, Oberpfaffenhofen, Germany

Key Points:

- Internal variability feedbacks better predict forced feedbacks in CMIP6 relative to CMIP5 by over 50%
- The improved prediction derives in part from the greater similarity between the patterns of internal and forced temperature changes in CMIP6
- The improved prediction does not significantly improve the emergent constraint associated with internal variability feedbacks

Supporting Information:

Supporting Information may be found in the online version of this article.

Correspondence to:

D. W. J. Thompson,
davet@atmos.colostate.edu

Citation:

Davis, L. L. B., Thompson, D. W. J., Rugenstein, M., & Birner, T. (2024). Links between internal variability and forced climate feedbacks: The importance of patterns of temperature variability and change. *Geophysical Research Letters*, *51*, e2024GL112774. https://doi.org/10.1029/2024GL112774

Received 27 SEP 2024
Accepted 16 NOV 2024

Abstract Understanding the relationships between internal variability and forced climate feedbacks is key for using observations to constrain future climate change. Here we probe and interpret the differences in these relationships between the climate change projections provided by the CMIP5 and CMIP6 experiment ensembles. We find that internal variability feedbacks better predict forced feedbacks in CMIP6 relative to CMIP5 by over 50%, and that the increased predictability derives primarily from the slow (>20 years) response to climate change. A key novel result is that the increased predictability is consistent with the higher resemblance between the patterns of internal and forced temperature changes in CMIP6, which suggests temperature pattern effects play a key role in predicting forced climate feedbacks. Despite the increased predictability, emergent constraints provided by observed internal variability are weak and largely unchanged from CMIP5 to CMIP6 due to the shortness of the observational record.

Plain Language Summary A key goal in climate change research is to use observed, internal climate feedbacks to constrain the forced feedbacks that govern climate change. Here the authors explore the differences in the relationships between internal and forced climate feedbacks in simulations run under the auspices of the two recent IPCC reports: The CMIP5 and CMIP6 simulations. They find notable increases in the relationships between internal and forced feedbacks between CMIP5 and CMIP6, and attribute these increases at least partially to the patterns of temperature variability associated with internal climate variability and forced climate change. However, they argue that the increases do not lead to improvements in our ability to constrain future climate change based on observations due to the uncertainty in the observed, internal climate feedbacks.

1. Introduction

A common approach to reducing uncertainty in climate change projections is to use observed internal variability to constrain the model-simulated feedbacks that govern the forced response to increasing greenhouse gas concentrations (e.g., Caldwell et al., 2018; Hall et al., 2019; Hall & Qu, 2006; He et al., 2021; Qu et al., 2018; Uribe et al., 2022, 2024; Williamson et al., 2021). Here we are motivated by the notable differences in climate change projections between the CMIP5 and CMIP6 experiments (e.g., Zelinka et al., 2020) to explore whether—and how—constraints imposed by the climate feedbacks associated with internal variability have likewise changed between the two sets of simulations (e.g., Rugenstein et al., 2023). We are interested in quantifying the changes in the relationships between internal climate feedbacks and forced climate feedbacks, the physical reasons for the changes, and the resulting implications for our ability to use observed internal variability to constrain climate change predictions. The results build on and extend several other studies that have probed internal climate feedbacks in the CMIP3, CMIP5, and CMIP6 ensembles individually (Colman & Hanson, 2013, 2017; Colman & Power, 2010, 2018; Dalton & Shell, 2013; Dessler, 2010, 2013; Dessler & Forster, 2018; He et al., 2021; Lutsko & Takahashi, 2018; Myers & Norris, 2015, 2016; Tsuchida et al., 2023a, Tsuchida, Mochizuki, Kawamura, & Kawano, 2023; Uribe et al., 2022, 2024; Zhou et al., 2015).

Throughout this study, we define β_λ as the linear relationship between (a) the amplitude of a given climate feedback λ in an unforced simulation of pre-industrial climate variability and (b) the amplitude of the same feedback in a forced simulation of abruptly quadrupled CO_2 concentrations by the same climate model. The study is framed around five guiding questions regarding the relationship β_λ between internal variability and forced climate feedbacks:

1. How does β_λ change between the climate models used in CMIP5 and CMIP6?
2. Does β_λ change between the early response (years 1–20) and late response (years 21–150) to idealized CO_2 forcing?
3. What feedback processes govern the differences in β_λ between the CMIP5 and CMIP6 simulations, and between the early and late responses to abrupt $4 \times CO_2$ forcing?
4. Is β_λ linked to the resemblance between the patterns of internal temperature variability and forced temperature change (i.e., is it influenced by temperature patterns effects)?
5. Do the differences in β_λ between the CMIP5 and CMIP6 simulations influence emergent constraints on future climate change—and thus our confidence in predictions—when observations are used to estimate the internal climate feedbacks?

Section 2 outlines the numerical models and methodology used in the study. Section 3 addresses the five guiding questions outlined above. In Section 4 we return to the above questions and discuss the implications of the results.

2. Models and Methodology

We use output from pre-industrial control and $4 \times CO_2$ experiments run on 30 models from CMIP5 and 59 models from CMIP6 (Supporting Tables S1, S2 in Supporting Information S1). The CMIP5 and CMIP6 pre-industrial experiments use constant radiative forcing agents representative of the period prior to the industrial revolution (Eyring et al., 2016; Taylor et al., 2012); the abrupt $4 \times CO_2$ experiments were branched from the pre-industrial experiments with an instantaneous, uniformly quadrupled CO_2 perturbation (Eyring et al., 2016; Taylor et al., 2012). All output is mapped onto a standard $5° \times 5°$ longitude-latitude grid using an area-conservative weighting scheme (Hanke et al., 2016).

We refer repeatedly to four principal quantities throughout the paper.

λ^I: The internal climate feedbacks derived from the pre-industrial experiments.
λ^F: The forced climate feedbacks derived from the abrupt $4 \times CO_2$ experiments.
β_λ: The inter-model linear relationship between λ^I and λ^F for a given CMIP ensemble.
Λ^I: The internal climate feedbacks estimated from detrended observations.

The model feedbacks are estimated using the regression methodology introduced by Gregory et al. (2004). Global-mean climate feedback parameters are found by regressing global-mean radiative flux anomalies (R) onto global-mean surface temperature anomalies (T):

$$\lambda = \frac{\overline{R'T'}}{\overline{T'^2}} \tag{1}$$

where R and T represent departures from the pre-industrial monthly climatology, overbars denote time-means, and primes denote deviations from the time-means. Spatially varying feedback parameters are found in a similar manner by regressing local radiative flux anomalies R_x against global average temperature anomalies T (e.g., Andrews et al., 2015; Hedemann et al., 2022):

$$\lambda_x = \frac{\overline{R_x'T'}}{\overline{T'^2}} \tag{2}$$

For each model, the internal variability feedbacks Λ^I are estimated from the first ensemble member of each pre-industrial experiment, and the forced feedbacks λ^F are estimated from the first ensemble member of each abrupt $4 \times CO_2$ experiment. We also calculate fast and slow components of the forced feedbacks by dividing the 150-year $4 \times CO_2$ experiments into early (years 1–20) and late (years 21–150) periods (Andrews et al., 2015; Geoffroy et al., 2013; Held et al., 2010). For the forced climate feedbacks, we use annual-average anomalies in order to avoid non-linearities arising from the strong projection of the forced response onto the seasonal cycle (not shown). For the internal variability feedbacks, in order to match the methodology required for observations, we (a) use averages of 11 successive 292-month (≈24-year) regressions from the first 150 years of each simulation (overlapping periods by 12 years, and with each period starting in March), and (b) use monthly anomalies formed by subtracting monthly 24-year climatologies from each regression period. Results based on single 150-year regressions and/or 150-year climatologies are qualitatively similar (not shown; see also Dalton & Shell, 2013). The relationships β_λ between λ^I and λ^F are found by regressing the model-dependent (time invariant) values of λ^F onto the corresponding model-dependent values of λ^I, that is:

$$\beta_\lambda = \frac{\left[\lambda^{F*}\lambda^{I*}\right]}{\left[\left(\lambda^{I*}\right)^2\right]} \tag{3}$$

where brackets denote weighted multi-model averages across the CMIP5 or CMIP6 model simulations (see below), and asterisks denote departures from the multi-model averages.

In the case of observations, the internal climate feedbacks λ^I are estimated by applying the regression methodology in Equation 1 to (a) global-average CERES EBAF top-of-the-atmosphere (TOA) radiative flux anomalies R (Loeb et al., 2018) and (b) global-average HadCRUT5 surface temperature anomalies T (Morice et al., 2021) over the period March 2000 to June 2024. In order to reduce the regression uncertainty, we use monthly anomalies instead of annual anomalies. We form the R and T anomalies by (a) subtracting their 24-year monthly climatologies then (b) removing the long-term linear trend from each result (in order to minimize the signals of radiative forcing and forced climate change in the observational record). In practice, similar results are obtained if we subtract from the CERES TOA radiative flux an explicit, annually resolved estimate of the historical radiative forcing (Dessler & Forster, 2018). The regression uncertainty of the observational feedbacks represents the uncertainty due to internal variability. Notably, the regression uncertainty of the 24-year feedbacks from each pre-industrial simulation is similar in magnitude and significantly correlated with the spread of the feedback estimates across successive 24-year periods (not shown).

All inter-model statistics are calculated using an "institutional democracy" scheme which treats each group of model results from the same institute as an independent sample (Abramowitz et al., 2019; Leduc et al., 2016; Masson & Knutti, 2011). This approach reduces double counting biases, where the degrees of freedom on inter-model statistics are overestimated due to giving similar results from models with more published variants higher weight (Leduc et al., 2016; see also Supporting Text S2 in Supporting Information S1). This effect is particularly strong in CMIP6, where several institutes publish as many as four or five model variants (Table S2 in Supporting Information S1). We applied institutional democracy by weighting the results in our multi-model averages and inter-model regressions by the number of models available from their respective institutes (e.g., $[\lambda] = \Sigma_i w_i \lambda_i / \Sigma_i w_i$, where $w_i = 1/n_i$ are the model weights and n_i is the model count for the parent institute of model i; see Tables S1, S2 in Supporting Information S1). In practice, the most notable effect of using institutional democracy rather than model democracy is to increase the uncertainty of the regression estimators; the regression coefficients themselves are qualitatively similar (not shown).

3. Results

3.1. Differences Between Internal and Forced Feedbacks in CMIP5 and CMIP6 Climate Models

Figure 1 shows the regression coefficients from linear regressions of forced climate feedbacks (λ^F) against internal variability feedbacks (λ^I) across each of the CMIP5 (light shading) and CMIP6 (dark shading) multi-model ensembles. The individual feedbacks and their consistency with previous work are documented in Supporting Text S1 and Supporting Figures S1–S2 in Supporting Information S1. The line fits associated with the regression coefficients in Figure 1 are shown in Supporting Figures S3–S5 in Supporting Information S1. The first column of Figure 1a shows results for the net feedbacks. In the case of the CMIP5 models, the amplitude of the relationship between the net internal and forced feedbacks is $\beta_\lambda = 0.20\,\mathrm{W\,m^{-2}\,K^{-1}/W\,m^{-2}K^{-1}}$, the fit explains 12% ($r = 0.35$) of the inter-model dispersion in the forced feedbacks, and the regression coefficient is not statistically significant at the 95% level (see also Supporting Figure S3 in Supporting Information S1). In the CMIP6 models, the relationship between the internal and forced feedbacks is more robust. The amplitude of the relationship is more than twice as large as in the CMIP5 models ($\beta_\lambda = 0.36$), the fit explains 26% ($r = 0.51$) of the inter-model dispersion in the forced feedbacks, and the regression coefficient is statistically significant at the 95% level. This

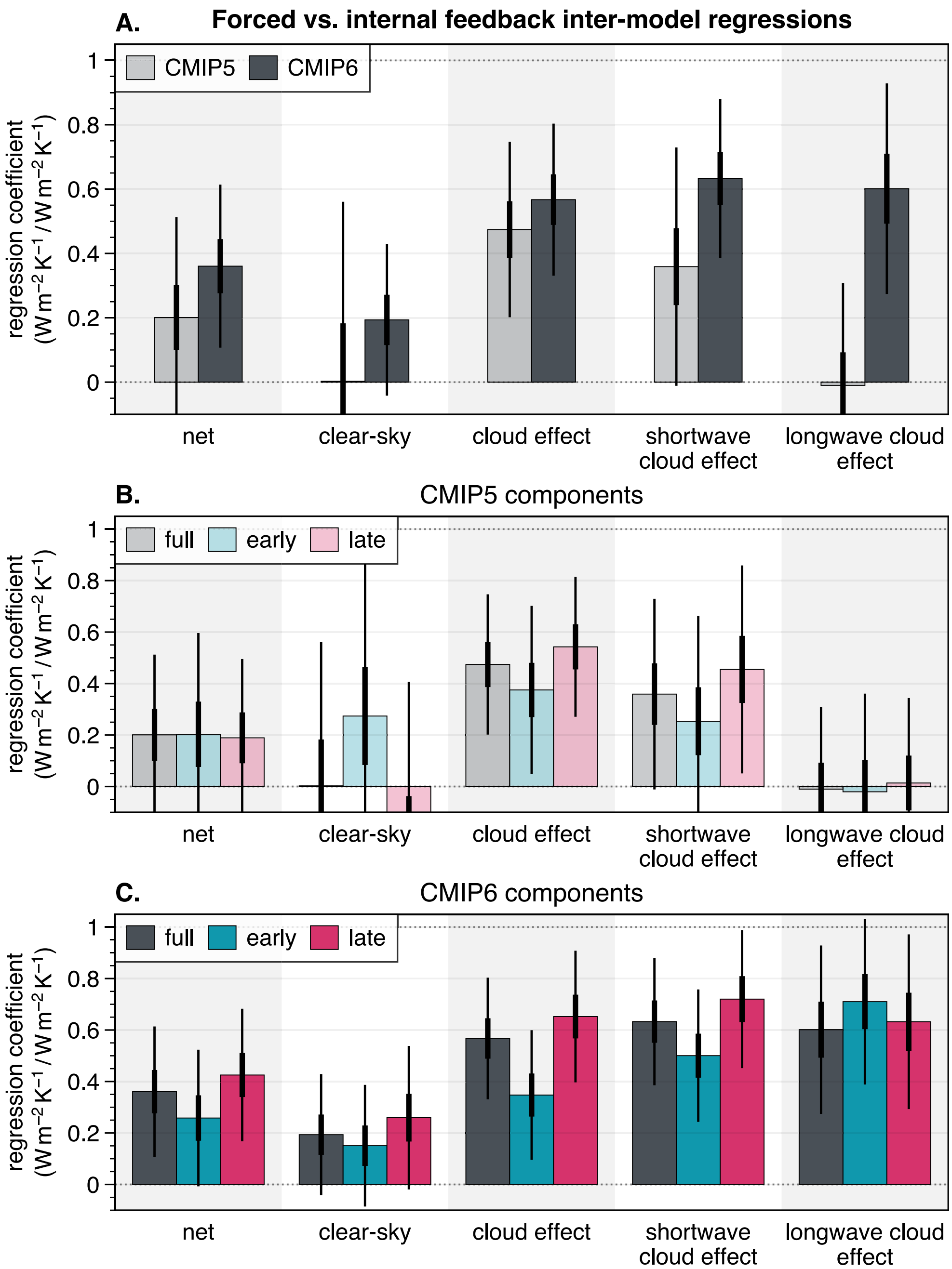

Figure 1. Relationships between forced and unforced climate feedbacks. Each background shading zone corresponds to the feedback component indicated on the x-axis. Bars indicate (institute-weighted) inter-model linear regression coefficients. Pale and dark shading indicate inter-model regressions across the CMIP5 and CMIP6 ensembles, respectively. Gray, blue, and pink shading indicate inter-model regressions against internal variability feedbacks using the full forced response (years 1–150), early forced response (years 1–20), and late forced response (years 21–150), respectively. Thin whiskers (thick whiskers) indicate the 95% (50%) uncertainty bounds for the regression coefficients according to two-sided student's t-tests.

contrasts notably with many other constraints on the forced response, which generally exhibit decreased strength in CMIP6 (Schlund et al., 2020).

The last four columns in Figure 1a decompose the results into components related to (a) clear-sky feedbacks λ_{CS} (calculated by regressing clear-sky radiative flux R_{CS} against surface temperature T) and (b) net, shortwave, and longwave cloud feedbacks λ_{CRE} (calculated by regressing the cloud radiative effect $CRE = R - R_{CS}$ against surface temperature T). The component β_λ values represent inter-model regressions of each forced feedback term (i.e., λ^F_{CS}, λ^F_{CRE}) against each internal variability counterpart (i.e., λ^I_{CS}, λ^I_{CRE}). We also estimated masking-adjusted cloud feedbacks using radiative kernels (Soden et al., 2008; Soden & Held, 2006), and the resulting β_λ coefficients were very similar to the results for cloud feedbacks without masking adjustments (Supporting Figure S6 in Supporting Information S1; see also Supporting Text S3 in Supporting Information S1). Thus, in order to simplify comparisons with observations, we use *CRE* to estimate cloud feedbacks for the rest of this paper. Note that the decompositions shown in Figure 1 are not linear; that is, in general, $\beta_{\lambda_{NET}} \neq \beta_{\lambda_{CS}} + \beta_{\lambda_{CRE}}$ since inter-model regressions of the feedback components $\lambda_{NET} = \lambda_{CS} + \lambda_{CRE}$ introduce cross terms (e.g., $\lambda^F_{CS} \cdot \lambda^I_{CRE}$) into the calculation of the regression coefficient in Equation 3. Nevertheless, the decomposition highlights (a) the climate feedback processes that are most closely related across internal and forced climate changes; and (b) the climate feedback processes that drive the largest differences in β_λ between CMIP5 and CMIP6.

Across both CMIP5 and CMIP6, the strength of the relationship between unforced internal variability and forced climate change is greater for cloud processes than for clear-sky processes (Figure 1a). Both processes lead to larger β_λ values in CMIP6 than in CMIP5: The inter-model regression coefficient increases from $\beta_\lambda = 0.47$ to 0.57 for cloud processes, and from zero to $\beta_\lambda = 0.19$ for clear-sky processes (see also Supporting Figure S3 in Supporting Information S1). The changes in cloud processes between CMIP5 and CMIP6 are much clearer when they are decomposed into their shortwave and longwave components. The shortwave cloud feedback regression coefficient nearly doubles from CMIP5 to CMIP6 ($\beta_\lambda = 0.36$ to 0.63; Figure 1a), and the variance explained by internal variability more than doubles from 24% to 53% (Supporting Figure S3 in Supporting Information S1). The longwave cloud feedback constraint is effectively zero in CMIP5 but is a notable $\beta_\lambda = 0.60$ in CMIP6, with 36% of the variance in the CMIP6 longwave cloud response explained by internal variability.

3.2. Differences Between Early and Late Feedbacks

We next decompose the differences in β_λ between the CMIP5 and CMIP6 ensembles into components driven by the early (fast) and late (slow) responses to the $4 \times CO_2$ perturbation, estimated by calculating forced feedbacks separately for years 1–20 and years 21–150 of the simulations (respectively). The gray and black bars in Figures 1b and 1c are reproduced from Figure 1a (respectively); the blue bars show results for the early period; and the red bars results for the late period. Across both CMIP5 and CMIP6, the late forced cloud feedbacks are more closely related to the internal variability feedbacks than the early forced cloud feedbacks (Figures 1b and 1c, center). That is, the internal variability of each model provides more information about its far-future cloud-radiative response to increasing CO_2 than its near-future response. The stronger β_λ relationships in CMIP6 relative to CMIP5 are also apparent for both the early and late periods (compare Figures 1b and 1c). The differences in β_λ between the CMIP5 and CMIP6 ensembles are generally more pronounced in the late response than the early response (see also Supporting Figures S4, S5 in Supporting Information S1). While the clear-sky feedbacks in CMIP5 are a notable exception (Figure 1b, center-left), this is partly due to the comparatively low inter-model spread of clear-sky feedbacks combined with the impact of two outlier models (see Supporting Figures S4–S5, B in Supporting Information S1).

3.3. Spatial Structure of the Relationships Between Internal and Forced Feedbacks

The results in Figure 1 indicate that the cloud component of the response to increasing CO_2 is more closely related to internal variability than the clear-sky response, with the individual shortwave and longwave components exhibiting much stronger inter-model relationships in CMIP6 compared to CMIP5. In Figure 2, we probe the spatial structures that underlie the differences in $\beta_{\lambda_{CRE}}$ between the CMIP5 and CMIP6 simulations (e.g., Caldwell et al., 2018). Results are again decomposed into the early and late responses to $4 \times CO_2$ perturbations. We first perform spatial decompositions of $\beta_{\lambda_{CRE}}$ by regressing local contributions to the global-mean forced cloud feedbacks (found using Equation 2) against the global-mean internal variability feedbacks shown in Figure 1a. The first two rows of Figure 2 show the resulting spatial patterns. Note that the global average of each pattern is equivalent to a bar shown in Figure 1 (e.g., the global-mean of Figure 2a is equivalent to the blue bar labeled *cloud effect* in Figure 1b). The key results of the decomposition are that (a) the positive inter-model regression coefficients $\beta_{\lambda_{CRE}}$ in Figure 1 derive mainly from tropical Pacific processes (Figures 2a–2b and 2d–2e, red shading); (b) the differences in $\beta_{\lambda_{CRE}}$ between CMIP5 and CMIP6 are most pronounced during the late period (consistent

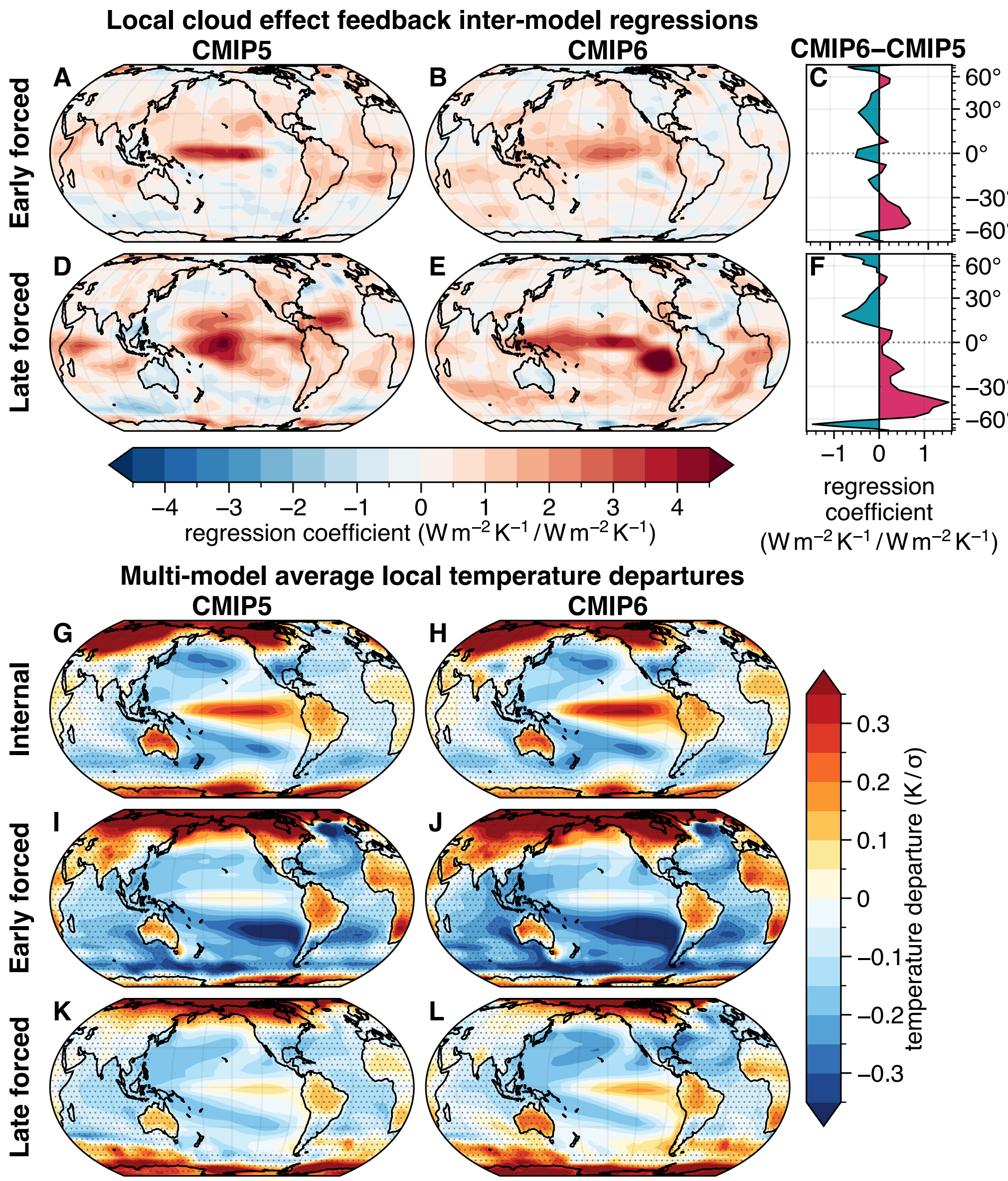

Figure 2. Local contributions to inter-model cloud feedback regressions and surface temperature change. The first and second columns indicate results for the CMIP5 and CMIP6 ensembles, respectively. The third column shows zonal-average differences between the first two columns. The upper panels indicate spatial decompositions of the cloud radiative effect feedback regression coefficients from Figure 1. Global averages of the upper first column (a, d) and the upper second column (b, e) are equivalent to bars from Figures 1B and 1C (respectively). The first and second rows show decompositions for the early (year 0–20) and late (year 21–150) forced responses to quadrupled CO_2, respectively. The lower panels indicate (institute-weighted) average surface temperature change. The third row shows local temperature departures associated with internal variability in global-average temperature (g, h). The fourth and fifth rows show local temperature departures from the global-average early (i, j) and late (k, l) forced responses, respectively. Stippling indicates regions excluded from the spatial projections (see text).

with Figures 1b and 1c, center); and (c) the differences in $\beta_{\lambda_{CRE}}$ during the late period arise from both the tropics (Figure 2f and 30°S to 10°N) and the Southern Ocean (Figure 2f and 60°S to 30°S; compare Figures 2d and 2e).

The differences in the regression patterns between the early response (Figures 2a and 2b) and the late response (Figures 2d and 2e) suggest a possible role for sea-surface temperature pattern effects in driving changes in $\beta_{\lambda_{CRE}}$. The last three rows of Figure 2 explore this role. The first of these rows shows the (institute-weighted) multi-model average relationships between local and global-mean temperature change in the unforced CMIP5 and

CMIP6 simulations (Figures 2g and 2h). That is, it shows the patterns of temperature change associated with *internal* variability in global-mean temperature. The results are formed from each control simulation by (a) subtracting the global-mean temperature anomaly T from every time step to form the departure field T_x^*, which is a function of grid point and time step and—by construction—has a spatial-mean of zero at each time step, then (b) projecting the departure time series T_x^* onto the global-mean time series T, that is: $\left(\overline{T_x^* \hat{T}}\right)_I$ where the overbar denotes the time mean, the subscript I denotes internal variability, and $\hat{T} = T/\sigma_I$ denotes the anomalous global-mean temperature normalized by its standard deviation σ_I. Across both CMIP5 and CMIP6, unforced variations in T are dominated by the eastern tropical Pacific. The bottom two rows show (institute-weighted) multi-model averages of the same temperature pattern metric calculated from the early (Figures 2i and 2j) and late (Figures 2k and 2l) components of the forced response to quadrupled CO_2. That is, they indicate the patterns of temperature change associated with *forced* changes in global-mean temperature. Here the results are formed by (a) subtracting the global-mean forced temperature response T at each time step to form the spatially varying component of the response T_x^* , then (b) projecting T_x^* onto the global-mean response T, that is: $\left(\overline{T_x^* \hat{T}}\right)_F$ where now the subscript F denotes the forced response and $\hat{T} = T/\sigma_F$ denotes the global-mean response normalized by its standard deviation σ_F. Note this metric is similar to the relative warming metric $\left(\overline{T_x T}\right)_F/\sigma_F^2$ used in other studies of time-evolving climate feedback processes (e.g., Andrews et al., 2018, 2022; Armour et al., 2013). Replacing our projection metrics with the relative warming metrics $\left(\overline{T_x T}\right)_I/\sigma_I^2$ and $\left(\overline{T_x T}\right)_F/\sigma_F^2$ yields qualitatively similar results (not shown).

We are interested in the similarities between (a) the unforced patterns of temperature variability (Figures 2g–2h) and (b) the forced patterns of temperature change (Figures 2i–2l). We are primarily concerned with similarities in the tropical Pacific, where the patterns of β_λ exhibit the largest differences between CMIP5 and CMIP6 (Figures 2a–2f). The *early* patterns of forced temperature change (Figures 2i and 2j) exhibit little structure in the tropical Pacific and thus bear little resemblance to the patterns of unforced temperature variability (Figures 2g and 2h). In contrast, the *late* forced patterns (Figures 2k and 2l) exhibit more distinct eastern tropical Pacific warming (see also Andrews et al., 2015, 2022) and thus bear greater resemblance to the unforced patterns.

The role of temperature patterns in driving changes in β_λ can be inferred by comparing spatial projections (i.e., cosine weighted inner products) of the patterns of forced temperature change onto the patterns of internal temperature variability. We compute projections using the patterns from each individual model, then take (institute-weighted) multi-model averages of the projections for each of the CMIP5 and CMIP6 ensembles. We also restrict each projection to the tropical and extratropical Pacific (i.e., ocean grid cells within 50°S–0°S 150°E−70°W, 0°N–10°N 125°E−70°W, and 10°N–50°N 125°E−100°W; stippling in Figures 2g–2l indicates the regions excluded). We denote $P(I, F_E)$ as the spatial projections of *early* forced temperature patterns onto internal variability temperature patterns; and $P(I, F_L)$ as the spatial projections of *late* forced patterns onto internal variability patterns. The key results are as follows: (a) The spatial projection $P(I, F_L)$ is about 85% larger than $P(I, F_E)$ for the CMIP6 simulations, but only 12% larger for the CMIP5 simulations; and (b) The spatial projection $P(I, F_L)$ is roughly 40% larger in CMIP6 than in CMIP5. The results are qualitatively similar when using (a) spatial correlation coefficients instead of spatial projections or b) scaled relative warming patterns instead of local temperature departures (see above). Quantitatively, the results thus indicate that the spatial similarities between the patterns of internal and forced temperature change are (a) higher in both CMIP5 and CMIP6 for the late period; and (b) larger in CMIP6 than CMIP5 during the late period. That the similarity between the patterns of internal and late forced temperature variability is more pronounced in CMIP6 suggests that the changes in β_λ between the two ensembles derive at least in part from the more pronounced similarities between internal patterns of temperature variability and forced patterns of temperature change over the key Pacific region.

3.4. Using the Relationships Between Internal and Forced Feedbacks as an Emergent Constraint

The relationships between internal and forced feedbacks can be combined with observational estimates of internal climate feedbacks to provide emergent constraints on forced climate feedbacks as follows (e.g., He et al., 2021; Lutsko et al., 2021; Lutsko & Takahashi, 2018; Uribe et al., 2022):

$$\Lambda^F = \left[\lambda^F\right] + \beta_\lambda\left(\Lambda^I - \left[\lambda^I\right]\right) \tag{4}$$

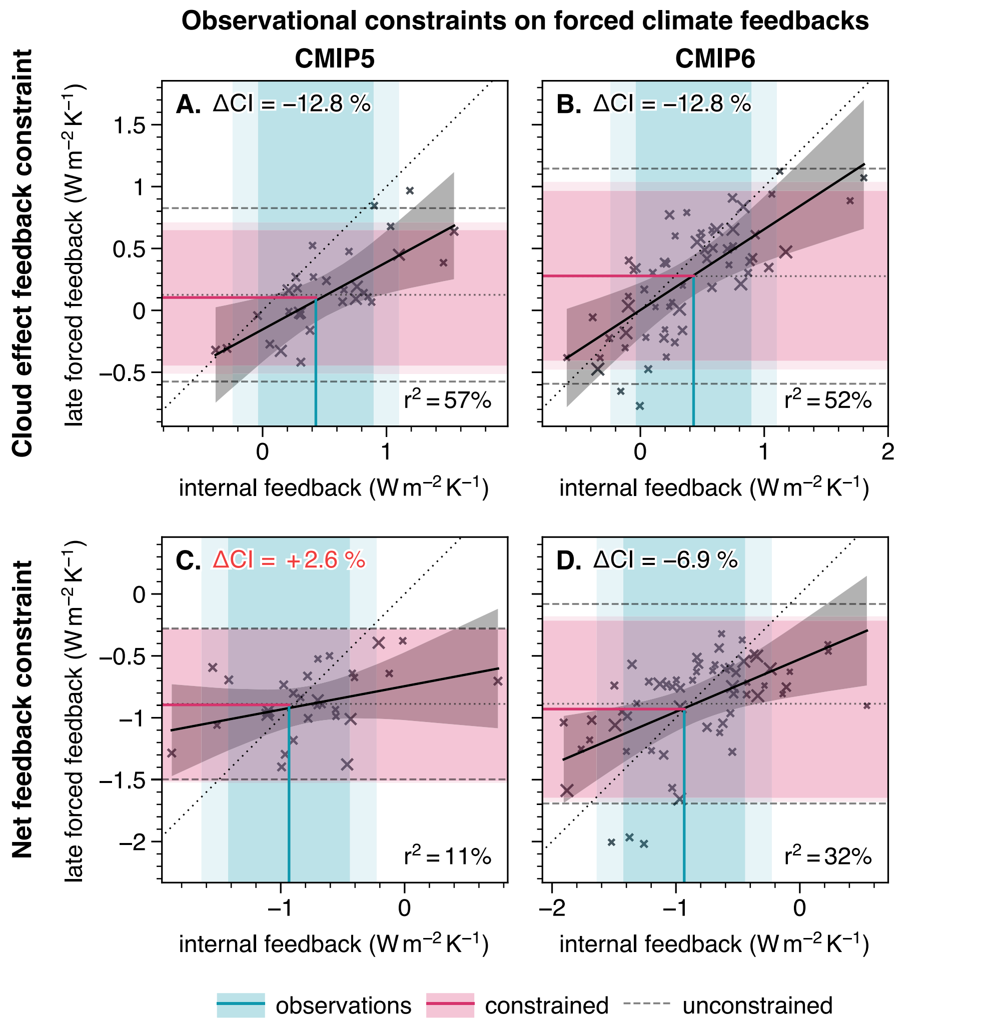

Figure 3. Emergent constraints on forced climate feedbacks using observed internal variability. The top row indicates constraints on the forced cloud radiative effect feedback. The bottom row indicates constraints on the total (net) forced climate feedback. The columns indicate results for the CMIP5 and CMIP6 ensembles, respectively. Gray markers indicate forced and internal climate feedbacks for individual models. Gray lines and shading indicate (institute-weighted) inter-model linear regressions and their 95% uncertainty bounds. The size of each marker is proportional to its weight in the regression (see text). Blue lines and shading indicate the mean and *t*-distributed 95% uncertainty bounds for the observational estimate of the corresponding internal variability feedback (see text). Pink lines and shading indicate the mean and 95% uncertainty bounds for the constrained estimate of the late forced climate feedback, accounting for both observational and regression uncertainty (see text). Horizontal gray dotted and dashed lines indicate (respectively) the mean and *t*-distributed 95% uncertainty bounds for the unconstrained forced feedbacks (i.e., *y*-coordinates of the gray markers). Lower right annotations indicate the percentage of (institute-weighted) variance in the forced feedbacks explained by each regression (i.e., the coefficient of determination r^2). Upper left annotations indicate the amount that each emergent constraint reduces inter-model spread in the response (i.e., the pink shading width minus the distance between the dashed gray lines). Positive values indicate unsuccessful constraints and are highlighted with red. The darker bands of blue and pink shading indicate the uncertainty associated with equivalent observational feedbacks derived from a hypothetical 50-year observing period instead of the true 292-month (≈24-year) period.

In the above, all parameters are as defined earlier, brackets indicate (institute-weighted) multi-model averages, and Λ^F is the observationally constrained forced climate feedback. Figure 3 shows the resulting emergent constraints on (A, B) the cloud component of the late forced climate feedback and (C, D) the net late climate feedback for each of the CMIP5 and CMIP6 ensembles. Both the cloud feedback constraint Λ^F_{CRE} and the net constraint Λ^F_{NET} are estimated with a bootstrapping procedure. The constraint methodology can be understood from Figure 3 as follows:

- The vertical blue lines and shading indicate (a) 292-month (≈24-year) observational estimates for the internal climate feedbacks Λ^I, and (b) their 95% uncertainty bounds, calculated from the t-distributions of the regression estimators (after replacing the degrees of freedom $n-2$ with $n_e = n(1-r_1)/(1+r_1) - 2$ to account for serial correlation r_1 in the regression residuals; Dessler & Forster, 2018, Thompson et al., 2015, Santer et al., 2000).
- The gray lines and shading indicate the inter-model regressions β_λ and their 95**%** uncertainty bounds (using the regression degrees of freedom $\hat{n}_e = \Sigma_i w_i - 2$, where w_i are the institutional democracy weights w_i; see also Equation 3, Supporting Figure S5 in Supporting Information S1).
- The horizontal pink lines and shading indicate the mean emergent constraints Λ^F and their 95% uncertainty bounds, arising from the propagation of the observational uncertainty (blue) through the regression uncertainty (gray). We estimate this combined uncertainty by (a) drawing 10^7 random samples from the observed Λ^I t-distribution, (b) applying Equation 4 using a random inter-model regression coefficient drawn from the t-distribution of β_λ, then (c) adding a random t-distributed error term scaled by the (institute-weighted) standard error of the regression s (e.g., Simpson et al., 2021).
- The horizontal dotted and dashed lines indicate the mean unconstrained forced climate feedbacks and their 95% uncertainty bounds, defined using a t-distribution with the (institute-weighted) sample mean and standard deviation from the y-coordinates of the markers.

Overall, the emergent constraints on forced climate feedbacks provided by Λ^I and β_λ are fairly weak (Figures 3a and 3b). Using the entire March 2000–June 2024 CERES period of record, observed internal variability reduces uncertainty in the forced cloud feedback λ^F_{CRE} by ≈13% for each of the CMIP5 and CMIP6 ensembles. The CERES observations also reduce the uncertainty in the net forced feedback λ^F by ≈7% for the CMIP6 ensemble, while the constraint is unsuccessful in CMIP5 (i.e., Λ^F is more uncertain than λ^F; Figures 3c and 3d). The modesty of the constraints arises mainly from the large uncertainty associated with the short 24-year observational record (see also Uribe et al., 2022). As indicated by the darker blue and pink shading in Figure 3, if the effective length of the record is increased to 50 years (i.e., the degrees of freedom of the regression are roughly doubled), then the observations reduce the uncertainty in the forced cloud feedback λ^F_{CRE} by ≈22% for both the CMIP5 and CMIP6 ensembles, and by ≈11% for the net forced feedback λ^F in CMIP6.

The cloud feedback constraints in Figure 3 are somewhat weaker than those reported He et al. (2021). This is most likely due to two steps in our observational methodology that were not used by He et al. (2021): (a) We detrend the observed temperature time series T and cloud radiative effect time series CRE before calculating regressions of CRE onto T; and (b) we account for serial correlation in the regression residual when estimating the degrees of freedom n_e used for our observational feedback uncertainty bounds. We prefer detrending the data in order to minimize the influence of anthropogenic forcing on our feedback regressions and to more directly target the internal variability component of the historical record. The fewer CMIP6 models available to He et al. (2021) at the time of their study also contribute to the increased constraint strength by producing a slightly higher β_{CRE} compared to the models in this study. We are able to approximately reproduce the strength of the He et al. (2021) constraint after adopting the above methodological choices (Supporting Figure S8 in Supporting Information S1; see also Supporting Text S4 in Supporting Information S1).

4. Conclusions

The observational record can be used to quantify the climate feedbacks associated with internal variability. However, observations are of limited use for directly quantifying the climate feedbacks associated with anthropogenic forcing, since (a) estimates of the forced feedback require an explicit estimate of historical radiative forcing, which is itself uncertain (e.g., Raghuraman et al., 2023; Smith & Forster, 2021); and (b) the CERES era provides only a single ≈24-year realization of the forced response to climate change, with a warming pattern that is notably distinct from model-simulated climate change (e.g., Marvel et al., 2018; Wills et al., 2022). As such, understanding the relationships between internal variability and forced climate feedbacks is essential for understanding the ability of observations to constrain future climate change.

Here we have quantified and interpreted the relationships between internal variability and forced climate feedbacks in the CMIP5 and CMIP6 experiment ensembles. A key novel result is that (a) the amplitude of the relationship between internal variability and forced climate feedbacks is consistent with (b) the degree of resemblance between the patterns of internal and forced temperature changes. That is, the amplitude of the relationship is linked to the temperature pattern effect. The role of the pattern effect is reminiscent of the "fluctuation-dissipation" perspective of the climate response to external forcing (e.g., Leith, 1975). For example, the atmospheric circulation response to external forcings—including those associated with climate change—projects most strongly onto the patterns of internal atmospheric variability that have the longest decorrelation times (Ring & Plumb, 2007, 2008). The patterns with the longest decorrelation times, in turn, arise as the leading patterns of internal climate variability since they explain the largest fraction of the variability in the climate system on monthly and longer timescales. The results shown here suggest that a similar mechanism acts to link the patterns of internal and forced temperature changes. Importantly, the differences in β_λ across time periods and ensembles are due to differences in the forced response rather than aliasing of internal variability into the forced signal; we obtain similar results if we explicitly remove interannual variations about the long-term trends from each quadrupled-CO_2 time series before regressing R against T (Supporting Figure S7 in Supporting Information S1; see also Supporting Text S3 in Supporting Information S1).

We close by addressing the five guiding questions outlined in the Introduction.

1. *How does β_λ change between the climate models used in CMIP5 and CMIP6?*

Internal variability feedbacks better predict forced feedbacks in CMIP6 relative to CMIP5. In terms of net feedbacks, the relationship between internal variability and the forced response is $\beta_\lambda = 0.20$ in CMIP5 but $\beta_\lambda = 0.36$ in CMIP6 (Figure 1a). The inter-model variance explained by internal variability feedbacks is only 12% in CMIP5, but 26% in CMIP6 (Supporting Figure S3 in Supporting Information S1).

2. *Does β_λ change between the early response (years 1–20) and late response (years 21–150) to idealized CO_2 forcing?*

Yes: β_λ is generally larger for the late response (years 21–150) to abruptly quadrupled CO_2 concentrations. Likewise, the increases in β_λ between the CMIP5 and CMIP6 simulations derive primarily from the late period (years 21–150) of the quadrupled CO_2 simulations.

3. *What feedback processes govern the differences in β_λ between the CMIP5 and CMIP6 simulations, and between the early and late responses to abrupt $4 \times CO_2$ forcing?*

The larger amplitudes of β_λ in CMIP6 arise from both the cloud and clear-sky components of the net climate feedback. Considered separately, both shortwave and especially longwave forced cloud feedbacks are much better constrained by internal variability in CMIP6 than in CMIP5. Taken together, the improvement is less striking due to compensation between shortwave and longwave feedbacks, but still reflects a modest increase from $\beta_\lambda = 0.47$ in CMIP5 to $\beta_\lambda = 0.57$ in CMIP6.

4. *Is β_λ linked to the resemblance between the patterns of internal temperature variability and forced temperature change (i.e., is it influenced by patterns effects)?*

Yes: The patterns of forced temperature change $\left(\overline{T_x^* \hat{T}}\right)_F$ bear greater resemblance to the patterns of internal temperature variability $\left(\overline{T_x^* \hat{T}}\right)_I$ in CMIP6 than in CMIP5. The resemblance to internal variability is also stronger in the late response than the early response. As such, the cloud feedbacks associated with the internal pattern effect are expected to better inform the cloud feedbacks associated with the long-term forced pattern effect in CMIP6.

5. *Do the differences in β_λ between the CMIP5 and CMIP6 simulations influence emergent constraints on future climate change—and thus our confidence in predictions—when observations are used to estimate the internal climate feedbacks?*

No: Not within the range of observational uncertainty (see also Uribe et al., 2022). The relationships between internal and forced cloud feedbacks (as given by $\beta_{\lambda_{CRE}}$) reduce the uncertainty of the forced cloud feedbacks by roughly 13%. However, there is no improvement in the constraint between CMIP5 and CMIP6 despite the modest increases in $\beta_{\lambda_{CRE}}$. The lack of improvement in the constraint arises from (a) the large uncertainty associated with the limited ≈24-year observational record and (b) the larger range of forced feedbacks in CMIP6. Interestingly: Both the CMIP5 and CMIP6 cloud feedback constraints remain modest even if the length of the observational record is assumed increased to 50 years. The implication is that it may not prove possible for many decades to constrain global forced feedbacks from observations of global internal variability using the emergent constraint framework. Alternative approaches based on individual cloud feedback mechanisms and spatially resolved cloud responses may instead prove more fruitful (e.g., Lutsko et al., 2021; Myers et al., 2021).

Data Availability Statement

The CMIP6 and CMIP5 data used in this study were obtained online via the Earth System Grid Federation (Cinquini et al., 2014). The software used to generate the results in this study are published under three separate repositories: One for calculating CMIP5 and CMIP6 feedbacks (Davis, 2024b), another for estimating observational climate feedbacks (Davis, 2024c), and a third for plotting and post-processing the results (Davis, 2024a). The Zelinka et al. (2020) forcing-feedback data used in Supporting Figure S2 in Supporting Information S1 were obtained from Zelinka (2021). The Huang et al. (2017) radiative kernels used in Supporting Figure S6 in Supporting Information S1 were obtained from Huang (2022). This work benefited from the open-source software packages Climate Data Operators (used to process model data; Schulzweida, 2023); Xarray (used to derive intermodel statistics; Hoyer et al., 2024); and Matplotlib, Cartopy, and Proplot (used to create the figures; Caswell et al., 2021; Elson et al., 2023; Davis, 2021).

Acknowledgments

We thank two anonymous reviewers for helpful and constructive reviews of the manuscript. We also thank Haozhe He for thoughtful discussion of the results. LLBD was supported by the National Science Foundation Climate and Large-Scale Dynamics (NSF CLD) Program under AGS-2116186 and DWJT's UK Royal Society Wolfson Fellowship. DWJT is supported by the National Aeronautics and Space Administration (NASA) under 80NSSC23K0113 and the NSF CLD Program under AGS-2116186. MR is funded by NASA under 80NSSC21K1042 and by NSF CLD under grant AGS-2233673.

References

Abramowitz, G., Herger, N., Gutmann, E., Hammerling, D., Knutti, R., Leduc, M., et al. (2019). ESD reviews: Model dependence in multi-model climate ensembles: Weighting, sub-selection and out-of-sample testing. *Earth System Dynamics*, *10*(1), 91–105. https://doi.org/10.5194/esd-10-91-2019

Andrews, T., Bodas-Salcedo, A., Gregory, J. M., Dong, Y., Armour, K. C., Paynter, D., et al. (2022). On the effect of historical SST patterns on radiative feedback. *Journal of Geophysical Research: Atmospheres*, *127*(18), e2022JD036675. https://doi.org/10.1029/2022JD036675

Andrews, T., Gregory, J. M., Paynter, D., Silvers, L. G., Zhou, C., Mauritsen, T., et al. (2018). Accounting for changing temperature patterns increases historical estimates of climate sensitivity. *Geophysical Research Letters*, *45*(16), 8490–8499. https://doi.org/10.1029/2018GL078887

Andrews, T., Gregory, J. M., & Webb, M. J. (2015). The dependence of radiative forcing and feedback on evolving patterns of surface temperature change in climate models. *Journal of Climate*, *28*(4), 1630–1648. https://doi.org/10.1175/JCLI-D-14-00545.1

Armour, K. C., Bitz, C. M., & Roe, G. H. (2013). Time-varying climate sensitivity from regional feedbacks. *Journal of Climate*, *26*(13), 4518–4534. https://doi.org/10.1175/JCLI-D-12-00544.1

Caldwell, P. M., Zelinka, M. D., & Klein, S. A. (2018). Evaluating emergent constraints on equilibrium climate sensitivity. *Journal of Climate*, *31*(10), 3921–3942. https://doi.org/10.1175/JCLI-D-17-0631.1

Caswell, T. A., Droettboom, M., Lee, A., De Andrade, E. S., Hoffmann, T., Hunter, J., et al. (2021). matplotlib/matplotlib: Rel: v3.4.3 [Software]. *Zenodo*. https://doi.org/10.5281/zenodo.5194481

Cinquini, L., Crichton, D., Mattmann, C., Harney, J., Shipman, G., Wang, F., et al. (2014). The Earth System Grid Federation: An open infrastructure for access to distributed geospatial data. *Future Generation Computer Systems*, *36*, 400–417. https://doi.org/10.1016/j.future.2013.07.002

Colman, R., & Hanson, L. (2017). On the relative strength of radiative feedbacks under climate variability and change. *Climate Dynamics*, *49*(5), 2115–2129. https://doi.org/10.1007/s00382-016-3441-8

Colman, R., & Power, S. B. (2018). What can decadal variability tell us about climate feedbacks and sensitivity? *Climate Dynamics*, *51*(9–10), 3815–3828. https://doi.org/10.1007/s00382-018-4113-7

Colman, R. A., & Hanson, L. I. (2013). On atmospheric radiative feedbacks associated with climate variability and change. *Climate Dynamics*, *40*(1–2), 475–492. https://doi.org/10.1007/s00382-012-1391-3

Colman, R. A., & Power, S. B. (2010). Atmospheric radiative feedbacks associated with transient climate change and climate variability. *Climate Dynamics*, *34*(7–8), 919–933. https://doi.org/10.1007/s00382-009-0541-8

Dalton, M. M., & Shell, K. M. (2013). Comparison of short-term and long-term radiative feedbacks and variability in twentieth-century global climate model simulations. *Journal of Climate*, *26*(24), 10051–10070. https://doi.org/10.1175/JCLI-D-12-00564.1

Davis, L. L. B. (2021). ProPlot (v0.9.5) [Software]. *Zenodo*. https://doi.org/10.5281/zenodo.5602155

Davis, L. L. B. (2024a). Open research: Climate feedback post-processing (v2.1.0) [Software]. *Zenodo*. https://doi.org/10.5281/zenodo.13905600

Davis, L. L. B. (2024b). Open research: CMIP5 and CMIP6 climate feedbacks (v2.1.0) [Software] [Dataset]. *Zenodo*. https://doi.org/10.5281/zenodo.13905597

Davis, L. L. B. (2024c). Open research: Observational climate feedbacks (v2.1.0) [Software] [Dataset]. *Zenodo*. https://doi.org/10.5281/zenodo.13905603

Dessler, A. E. (2010). A determination of the cloud feedback from climate variations over the past decade. *Science*, *330*(6010), 1523–1527. https://doi.org/10.1126/science.1192546

Dessler, A. E. (2013). Observations of climate feedbacks over 2000–10 and comparisons to climate models. *Journal of Climate*, *26*(1), 333–342. https://doi.org/10.1175/JCLI-D-11-00640.1

Dessler, A. E., & Forster, P. M. (2018). An estimate of equilibrium climate sensitivity from interannual variability. *Journal of Geophysical Research: Atmospheres*, *123*(16), 8634–8645. https://doi.org/10.1029/2018JD028481

Elson, P., de Andrade, E. S., Lucas, G., May, R., Hattersley, R., Campbell, E., et al. (2023). SciTools/cartopy: v0.22.0 (v0.22.0) [Software]. *Zenodo*. https://doi.org/10.5281/zenodo.8216315

Eyring, V., Bony, S., Meehl, G. A., Senior, C. A., Stevens, B., Stouffer, R. J., & Taylor, K. E. (2016). Overview of the coupled model intercomparison project phase 6 (CMIP6) experimental design and organization. *Geoscientific Model Development*, *9*(5), 1937–1958. https://doi.org/10.5194/gmd-9-1937-2016

Geoffroy, O., Saint-Martin, D., Bellon, G., Voldoire, A., Olivié, D. J. L., & Tytéca, S. (2013). Transient climate response in a two-layer energy-balance model. Part II: Representation of the efficacy of deep-ocean heat uptake and validation for CMIP5 AOGCMs. *Journal of Climate*, *26*(6), 1859–1876. https://doi.org/10.1175/JCLI-D-12-00196.1

Gregory, J. M., Ingram, W. J., Palmer, M. A., Jones, G. S., Stott, P. A., Thorpe, R. B., et al. (2004). A new method for diagnosing radiative forcing and climate sensitivity. *Geophysical Research Letters*, *31*(3), L03205. https://doi.org/10.1029/2003GL018747

Hall, A., Cox, P., Huntingford, C., & Klein, S. (2019). Progressing emergent constraints on future climate change. *Nature Climate Change*, *9*(4), 269–278. https://doi.org/10.1038/s41558-019-0436-6

Hall, A., & Qu, X. (2006). Using the current seasonal cycle to constrain snow albedo feedback in future climate change. *Geophysical Research Letters*, *33*(3), L03502. https://doi.org/10.1029/2005GL025127

Hanke, M., Redler, R., Holfeld, T., & Yastremsky, M. (2016). Yac 1.2.0: New aspects for coupling software in earth system modelling. *Geoscientific Model Development*, *9*(8), 2755–2769. https://doi.org/10.5194/gmd-9-2755-2016

He, H., Kramer, R. J., & Soden, B. J. (2021). Evaluating observational constraints on intermodel spread in cloud, temperature, and humidity feedbacks. *Geophysical Research Letters*, *48*(17), e2020GL092309. https://doi.org/10.1029/2020GL092309

Hedemann, C., Mauritsen, T., Jungclaus, J., & Marotzke, J. (2022). Reconciling conflicting accounts of local radiative feedbacks in climate models. *Journal of Climate*, *35*(10), 3131–3146. https://doi.org/10.1175/JCLI-D-21-0513.1

Held, I. M., Winton, M., Takahashi, K., Delworth, T., Zeng, F., & Vallis, G. K. (2010). Probing the fast and slow components of global warming by returning abruptly to preindustrial forcing. *Journal of Climate*, *23*(9), 2418–2427. https://doi.org/10.1175/2009JCLI3466.1

Hoyer, S., Roos, M., Joseph, H., Magin, J., Cherian, D., Fitzgerald, C., et al. (2022). Xarray (v0.21.0) [Software]. *Zenodo*. https://doi.org/10.5281/zenodo.5914998

Huang, Y. (2022). ERA-interim reanalysis based radiative kernels (v1) [Dataset]. *Mendeley Data*. https://doi.org/10.17632/3drx8fmmz9.1

Huang, Y., Xia, Y., & Tan, X. (2017). On the pattern of CO2 radiative forcing and poleward energy transport. *Journal of Geophysical Research: Atmospheres*, *122*(20), 578–593. https://doi.org/10.1002/2017JD027221

Leduc, M., Laprise, R., de Elía, R., & Šeparović, L. (2016). Is institutional democracy a good proxy for model independence? *Journal of Climate*, *29*(23), 8301–8316. https://doi.org/10.1175/JCLI-D-15-0761.1

Leith, C. E. (1975). Climate response and fluctuation dissipation. *Journal of the Atmospheric Sciences*, *32*(10), 2022–2026. https://doi.org/10.1175/1520-0469(1975)032<2022:CRAFD>2.0.CO;2

Loeb, N. G., Doelling, D. R., Wang, H., Su, W., Nguyen, C., Corbett, J. G., et al. (2018). Clouds and the earth's radiant energy system (CERES) energy balanced and filled (EBAF) top-of-atmosphere (TOA) edition-4.0 data product. *Journal of Climate*, *31*(2), 895–918. https://doi.org/10.1175/JCLI-D-17-0208.1

Lutsko, N. J., Popp, M., Nazarian, R. H., & Albright, A. L. (2021). Emergent constraints on regional cloud feedbacks. *Geophysical Research Letters*, *48*(10), e2021GL092934. https://doi.org/10.1029/2021GL092934

Lutsko, N. J., & Takahashi, K. (2018). What can the internal variability of CMIP5 models tell us about their climate sensitivity? *Journal of Climate*, *31*(13), 5051–5069. https://doi.org/10.1175/JCLI-D-17-0736.1

Marvel, K., Pincus, R., Schmidt, G. A., & Miller, R. L. (2018). Internal variability and disequilibrium confound estimates of climate sensitivity from observations. *Geophysical Research Letters*, *45*(3), 1595–1601. https://doi.org/10.1002/2017GL076468

Masson, D., & Knutti, R. (2011). Climate model genealogy. *Geophysical Research Letters*, *38*(8), L08703. https://doi.org/10.1029/2011GL046864

Morice, C. P., Kennedy, J. J., Rayner, N. A., Winn, J. P., Hogan, E., Killick, R. E., et al. (2021). An updated assessment of near-surface temperature change from 1850: The HadCRUT5 data set. *Journal of Geophysical Research: Atmospheres*, *126*(3), e2019JD032361. https://doi.org/10.1029/2019JD032361

Myers, T. A., & Norris, J. R. (2015). On the relationships between subtropical clouds and meteorology in observations and CMIP3 and CMIP5 models. *Journal of Climate*, *28*(8), 2945–2967. https://doi.org/10.1175/JCLI-D-14-00475.1

Myers, T. A., & Norris, J. R. (2016). Reducing the uncertainty in subtropical cloud feedback. *Geophysical Research Letters*, *43*(5), 2144–2148. https://doi.org/10.1002/2015GL067416

Myers, T. A., Scott, R. C., Zelinka, M. D., Klein, S. A., Norris, J. R., & Caldwell, P. M. (2021). Observational constraints on low cloud feedback reduce uncertainty of climate sensitivity. *Nature Climate Change*, *11*(6), 1–7. https://doi.org/10.1038/s41558-021-01039-0

Qu, X., Hall, A., DeAngelis, A. M., Zelinka, M. D., Klein, S. A., Su, H., et al. (2018). On the emergent constraints of climate sensitivity. *Journal of Climate*, *31*(2), 863–875. https://doi.org/10.1175/JCLI-D-17-0482.1

Raghuraman, S. P., Paynter, D., Menzel, R., & Ramaswamy, V. (2023). Forcing, cloud feedbacks, cloud masking, and internal variability in the cloud radiative effect satellite record. *Journal of Climate*, *36*(12), 1–38. https://doi.org/10.1175/JCLI-D-22-0555.1

Ring, M. J., & Plumb, R. A. (2007). Forced annular mode patterns in a simple atmospheric general circulation model. *Journal of the Atmospheric Sciences*, *65*(10), 3611–3626. https://doi.org/10.1175/JAS4031.1

Ring, M. J., & Plumb, R. A. (2008). The response of a simplified GCM to axisymmetric forcings: Applicability of the fluctuation–dissipation theorem. *Journal of the Atmospheric Sciences*, *65*(12), 3880–3898. https://doi.org/10.1175/2008JAS2773.1

Rugenstein, M., Dhame, S., Olonscheck, D., Wills, R. J., Watanabe, M., & Seager, R. (2023). Connecting the SST pattern problem and the hot model problem. *Geophysical Research Letters*, *50*(22), e2023GL105488. https://doi.org/10.1029/2023GL105488

Santer, B. D., Wigley, T. M. L., Boyle, J. S., Gaffen, D. J., Hnilo, J. J., Nychka, D., et al. (2000). Statistical significance of trends and trend differences in layer-average atmospheric temperature time series. *Journal of Geophysical Research*, *105*(D6), 7337–7356. https://doi.org/10.1029/1999JD901105

Schlund, M., Lauer, A., Gentine, P., Sherwood, S. C., & Eyring, V. (2020). Emergent constraints on equilibrium climate sensitivity in CMIP5: Do they hold for CMIP6? *Earth System Dynamics Discussions*(July), 1–40. https://doi.org/10.5194/esd-2020-49

Schulzweida, U. (2023). CDO user guide [Software]. *Zenodo*. https://doi.org/10.5281/zenodo.1435454

Simpson, I. R., McKinnon, K. A., Davenport, F. V., Tingley, M., Lehner, F., Al Fahad, A., & Chen, D. (2021). Emergent constraints on the large-scale atmospheric circulation and regional hydroclimate: Do they still work in CMIP6 and how much can they actually constrain the future? *Journal of Climate*, *34*(15), 6355–6377. https://doi.org/10.1175/JCLI-D-21-0055.1

Smith, C. J., & Forster, P. M. (2021). Suppressed late-20th century warming in CMIP6 models explained by forcing and feedbacks. *Geophysical Research Letters*, *48*(19), e2021GL094948. https://doi.org/10.1029/2021GL094948

Soden, B. J., & Held, I. M. (2006). An assessment of climate feedbacks in coupled ocean–atmosphere models. *Journal of Climate*, *19*(14), 3354–3360. https://doi.org/10.1175/JCLI3799.1

Soden, B. J., Held, I. M., Colman, R., Shell, K. M., Kiehl, J. T., & Shields, C. A. (2008). Quantifying climate feedbacks using radiative kernels. *Journal of Climate*, *21*(14), 3504–3520. https://doi.org/10.1175/2007JCLI2110.1

Taylor, K. E., Stouffer, R. J., & Meehl, G. A. (2012). An overview of CMIP5 and the experiment design. *Bulletin of the American Meteorological Society*, *93*(4), 485–498. https://doi.org/10.1175/BAMS-D-11-00094.1

Thompson, D. W. J., Barnes, E. A., Deser, C., Foust, W. E., & Phillips, A. S. (2015). Quantifying the role of internal climate variability in future climate trends. *Journal of Climate*, *28*(16), 6443–6456. https://doi.org/10.1175/JCLI-D-14-00830.1

Tsuchida, K., Mochizuki, T., Kawamura, R., & Kawano, T. (2023). Interdecadal variations of radiative feedbacks associated with the El Niño and Southern Oscillation (ENSO) in CMIP6 models. *Geophysical Research Letters*, *50*(23), e2023GL106127. https://doi.org/10.1029/2023GL106127

Tsuchida, K., Mochizuki, T., Kawamura, R., Kawano, T., & Kamae, Y. (2023). Diversity of lagged relationships in global means of surface temperatures and radiative budgets for CMIP6 piControl simulations. *Journal of Climate*, *36*(24), 8743–8759. https://doi.org/10.1175/JCLI-D-23-0045.1

Uribe, A., Bender, F., & Mauritsen, T. (2024). Constraining net long term climate feedback from satellite observed internal variability possible by mid 2030s. https://doi.org/10.5194/egusphere-2024-1559

Uribe, A., Bender, F. A.-M., & Mauritsen, T. (2022). Observed and CMIP6 modeled internal variability feedbacks and their relation to forced climate feedbacks. *Geophysical Research Letters*, *49*(24), e2022GL100075. https://doi.org/10.1029/2022GL100075

Williamson, M. S., Thackeray, C. W., Cox, P. M., Hall, A., Huntingford, C., & Nijsse, F. J. M. M. (2021). Emergent constraints on climate sensitivities. *Reviews of Modern Physics*, *93*(2), 025004. https://doi.org/10.1103/RevModPhys.93.025004

Wills, R. C. J., Dong, Y., Proistosecu, C., Armour, K. C., & Battisti, D. S. (2022). Systematic climate model biases in the large-scale patterns of recent sea-surface temperature and sea-level pressure change. *Geophysical Research Letters*, *49*(17), e2022GL100011. https://doi.org/10.1029/2022GL100011

Zelinka, M. D. (2021). mzelinka/cloud-radiative-kernels: Sep 17, 2021 Release (v1.0) [Dataset]. *Zenodo*. https://doi.org/10.5281/zenodo.5514137

Zelinka, M. D., Myers, T. A., McCoy, D. T., Po-Chedley, S., Caldwell, P. M., Ceppi, P., et al. (2020). Causes of higher climate sensitivity in CMIP6 models. *Geophysical Research Letters*, *47*(1), e2019GL085782. https://doi.org/10.1029/2019GL085782

Zhou, C., Zelinka, M. D., Dessler, A. E., & Klein, S. A. (2015). The relationship between interannual and long-term cloud feedbacks. *Geophysical Research Letters*, *42*(23), 10–69. https://doi.org/10.1002/2015GL066698